An Energy-Based Model of Longitudinal Splitting in Unidirectional Fiber-Reinforced Composites

K. Oguni

G. Ravichandran
Mem. ASME

Graduate Aeronautical Laboratories,
California Institute of Technology,
Pasadena, CA 91125

Unidirectional fiber-reinforced composites are often observed to fail in a longitudinal splitting mode in the fiber direction under far-field compressive loading with weak lateral confinement. An energy-based model is developed based on the principle of minimum potential energy and the evaluation of effective properties to obtain an analytical approximation to the critical stress for longitudinal splitting. The analytic estimate for the compressive strength is used to illustrate its dependence on material properties, surface energy, fiber volume fraction, fiber diameter, and lateral confining pressure. The predictions of the model show good agreement with available experimental data.
[S0021-8936(00)02003-1]

1 Introduction

Fiber-reinforced composite materials are used in the form of laminates in numerous structural applications by taking advantage of their directional properties. Such applications are often limited by the compressive strength of the composite materials that are used. Failure modes in composite laminates are complex and are not always easily understood (e.g., [1,2]). On the other hand, unidirectional fiber-reinforced composites serve as excellent model materials for investigating the associated strength and failure issues. Unidirectional fiber-reinforced composites also have much lower compressive strength than their tensile strength for loading in the fiber direction. Therefore, the prediction of the compressive strength is a critical issue in designing composite materials and composite structures. Commonly observed failure modes in unidirectional composites under compression in the fiber direction include (i) longitudinal or axial splitting due to transverse cracking, (ii) fiber kinking (initiation and propagation of kink bands or microbuckles), and (iii) longitudinal splitting followed by fiber kinking (see for e.g., [2,3]). These failure modes are also observed under axial compression in the presence of lateral confinement. However, the mechanisms, which govern these failure modes in composites, are not completely understood. The effect of lateral confinement on compressive strength is an outstanding issue because of its relevance in developing and validating existing phenomenological failure models for composites (e.g., [4,5]). Also, in composite laminates, even under uniaxial compression, the stress state is multiaxial, and hence there is a need for models that can reliably predict their strength under multiaxial stress states. For the kinking mode of failure, a wide range of experimental, analytical, computational efforts have been undertaken (e.g., [2,3,6–9]). On the other hand, relatively little is known about longitudinal splitting due to transverse cracking. A number of researchers have observed an increase in the compressive strength with increasing lateral confinement (e.g., [10–12]). Further, from a materials design point of view, it is desirable to have models that can predict the strength of the composites in terms of the properties of fiber, matrix, and their interface. Motivated by these experimental observations and the current lack of satisfactory models for longitudinal (axial) splitting in composites (with an exception in the work by [9]), a new energy-based approach for predicting compressive strength of unidirectional fiber reinforced composites has been developed and is presented here.

One way to investigate the longitudinal splitting under compression is to compute the energy release rate and track the evolution of dominant microcracks in the composites. However, the stress field and the evolution law for a crack embedded in a highly heterogeneous material such as fiber-reinforced composites is extremely complicated and hence a satisfactory analytic approach appears not to be plausible in this case. In this paper, an energetic approach similar to the one that has been used for studying axial splitting in isotropic brittle solids such as ceramics ([13]) is employed to gain insights into longitudinal splitting phenomena in fiber-reinforced composites. By combining the principle of minimum potential energy and the effective properties of the composite, an energy-based criterion for longitudinal splitting of unidirectional fiber-reinforced composite is established. Hashin [14] has used a similar approach in determining the energy release rate for fracture in laminated composites.

Due to the heterogeneity and anisotropy of the fiber-reinforced composite, excessive elastic energy is stored in the composite under compression. Longitudinal splitting can be regarded as a process in which the excessive elastic energy is released through the formation of new surfaces. Therefore, when the reduction of the stored elastic energy by splitting compensates the surface energy, the specimen splits. This energy-based failure criterion combined with the effective properties of the composite based on the elastic properties of the matrix and the fiber provides an analytical expression for the critical stress (compressive strength) for longitudinal splitting. This expression illustrates the effect of material properties, surface energy, fiber volume fraction, fiber diameter, and lateral confining pressure on the critical axial compressive stress for longitudinal splitting. The model predictions are compared with available experimental results in the literature ([10,11,15]) and show good agreement. The predictions break down for large confining pressures due to failure mode transition to kinking which is not accounted for in the present model.

Contributed by the Applied Mechanics Division of THE AMERICAN SOCIETY OF MECHANICAL ENGINEERS for publication in the ASME JOURNAL OF APPLIED MECHANICS. Manuscript received by the ASME Applied Mechanics Division, June 9, 1999; final revision, Dec. 7, 1999. Associate Technical Editor: K. T. Ramesh. Discussion on the paper should be addressed to the Technical Editor, Professor Lewis T. Wheeler, Department of Mechanical Engineering, University of Houston, Houston, TX 77204-4792, and will be accepted until four months after final publication of the paper itself in the ASME JOURNAL OF APPLIED MECHANICS.

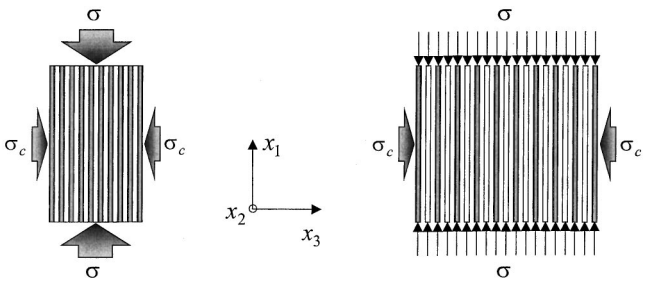

(a) Unsplit (b) Totally Split

Fig. 1 Schematics of unsplit and longitudinally split configurations of a unidirectional fiber composite

2 Energy-Based Model for Longitudinal Splitting

2.1 Problem Formulation. Consider a cylindrical specimen of an ideal[1] unidirectional fiber-reinforced composite under lateral confining stress, σ_c, and axial compressive stress, σ, shown schematically in Fig. 1(*a*). Under this setting, compare two configurations shown in Fig. 1: (*a*) one is unsplit, and (*b*) the other is totally split in the fiber direction. Let the total potential energy density of unsplit and split specimen be Π_u and Π_s, respectively. Comparison between Π_u and Π_s provides the critical axial stress for splitting under given lateral confining stress, σ_c. The criterion for longitudinal splitting is the minimization of the total potential energy density of the specimen. In other words, when Π_u exceeds Π_s, the specimen splits ([13]).

The total potential energy is computed in terms of the effective material properties as a function of the properties of fiber and matrix using the concept of representative volume element (RVE). Instead of considering the entire problem, an auxiliary problem is set up focusing on an element (RVE) which consists of a fiber surrounded by the matrix according to the volume fraction under the same strain or stress boundary condition as that of the original problem. If the specimen is macroscopically homogeneous, the average strain and stress over the RVE are the same as that of the entire specimen. In the problem under consideration, because of the random in-plane distribution of the fibers, the RVE reduces to a circular cylinder which consists of a single straight fiber of the specimen length surrounded with matrix according to the fiber volume fraction. The issues related to establishing RVEs in fiber-reinforced composites are well established (e.g., [16–18]).

2.2 Energy Criterion for Longitudinal Splitting

2.2.1 Total Potential Energy of Unsplit Specimen. The total potential energy density of the unsplit specimen, Π_u, is the same as the elastic energy density. Hence, under stress (traction) boundary condition, Π_u is given as follows:

$$\Pi_u=\frac{1}{V}\int_V\left\{\frac{1}{2}\boldsymbol{\varepsilon}(x):\mathbf{C}(x):\boldsymbol{\varepsilon}(x)-\boldsymbol{\sigma}(x):\boldsymbol{\varepsilon}(x)\right\}dx$$

$$=\frac{1}{V}\int_V\left\{-\frac{1}{2}\boldsymbol{\sigma}(x):\mathbf{S}(x):\boldsymbol{\sigma}(x)\right\}dx=-\frac{1}{2}\overline{\boldsymbol{\sigma}}:\mathbf{S}_*:\overline{\boldsymbol{\sigma}} \tag{2.1}$$

where V is the volume of the RVE, $\mathbf{C}(x)$ and $\mathbf{S}(x)$ are the fourth-order elasticity and compliance tensors at point $\boldsymbol{x}$, respectively, $\boldsymbol{\varepsilon}(x)$ is the strain field, $\boldsymbol{\sigma}(x)$ is the stress field, and $\overline{\boldsymbol{\sigma}}$ is the volumetric average stress tensor over V which corresponds to the prescribed stress on the boundary of the specimen. $\mathbf{S}_*$ is the effective compliance tensor of the unsplit specimen.

[1]The fibers of the same diameter are aligned and homogeneously distributed in the plane (x_2-x_3) perpendicular (transverse) to the fiber direction (x_1).

Because of the unidirectional reinforcement of the fibers, the specimen is transversely isotropic. Besides, the cartesian coordinates, x_1, x_2, and x_3 directions are also the principal directions. Therefore, to evaluate Π_u, we need only four independent effective moduli, namely, the longitudinal Young's modulus, E_1^*, Poisson ratio, ν_{21}^*, the plane strain bulk modulus, K_{23}^* and the shear modulus, G_{23}^*. Using the cylindrical RVE introduced before, effective elastic moduli of the unidirectional composite for random in-plane distribution of fibers, $E_1^*, \nu_{21}^*, K_{23}^*$, and the upper and lower bounds for G_{23}^* have been obtained by Hashin and Rosen [16]. Since the lower bound corresponds to the macro-stress prescribed problem, the lower bound for G_{23}^* is used here. The expressions for the moduli tensor and related elasticity constants are shown in the Appendix in terms of the elastic constants of the fiber and the matrix as well as their volume fractions.

The average stress-strain relation for the RVE is given as follows:[2]

$$\begin{aligned}\overline{\sigma}_{11}&=C_{11}^*\overline{\varepsilon}_{11}+C_{12}^*\overline{\varepsilon}_{22}+C_{12}^*\overline{\varepsilon}_{33}\\ \overline{\sigma}_{22}&=C_{12}^*\overline{\varepsilon}_{11}+C_{22}^*\overline{\varepsilon}_{22}+C_{23}^*\overline{\varepsilon}_{33}\\ \overline{\sigma}_{33}&=C_{12}^*\overline{\varepsilon}_{11}+C_{23}^*\overline{\varepsilon}_{22}+C_{22}^*\overline{\varepsilon}_{33}\end{aligned} \tag{2.2}$$

The prescribed stress boundary conditions are

$$\overline{\sigma}_{11}=-\sigma \quad \overline{\sigma}_{22}=\overline{\sigma}_{33}=-\sigma_c \quad \overline{\sigma}_{12}=\overline{\sigma}_{13}=\overline{\sigma}_{23}=0 \tag{2.3}$$

where σ and σ_c are the magnitudes of the axial stress and the lateral confinement. Compressive stress components are assumed to be negative. The total potential energy density for the unsplit specimen, Π_u, is a quadratic form of the compressive stress, σ,

$$\begin{aligned}\Pi_u&=-\frac{1}{2}\begin{bmatrix}-\sigma\\-\sigma_c\\-\sigma_c\end{bmatrix}^T\begin{bmatrix}C_{11}^* & C_{12}^* & C_{12}^*\\ C_{12}^* & C_{22}^* & C_{23}^*\\ C_{12}^* & C_{23}^* & C_{22}^*\end{bmatrix}^{-1}\begin{bmatrix}-\sigma\\-\sigma_c\\-\sigma_c\end{bmatrix}\\ &=\frac{(C_{22}^*+C_{23}^*)\sigma^2-4C_{12}^*\sigma_c\sigma+2C_{11}^*\sigma_c^2}{4C_{12}^{*2}-2C_{11}^*(C_{22}^*+C_{23}^*)}\\ &=-\frac{1}{2}\left\{\frac{\sigma^2}{E_1^*}+\frac{4\nu_{21}^*\sigma_c\sigma}{E_1^*}+\left(\frac{1}{K_{23}^*}+\frac{4\nu_{21}^{*2}}{E_1^*}\right)\sigma_c^2\right\}.\end{aligned} \tag{2.4}$$

2.2.2 Total Potential Energy of Split Specimen. Under the same boundary condition as that of the unsplit specimen (2.3) and assuming that *each* RVE splits at the boundary of the matrix and the fiber, i.e., the split is caused by an interfacial crack (delamination), the split RVE can be regarded as two columns, consisting of either the fiber or the matrix. Such a simplifying assumption enables gaining insights into the strength of composites. The elastic energy density of the RVE after splitting, E_s, is given by

$$E_s=\frac{1}{V}\int_V\left\{-\frac{1}{2}\boldsymbol{\sigma}(x):\mathbf{S}(x):\boldsymbol{\sigma}(x)\right\}dx$$

$$=-\frac{1}{2}\overline{\boldsymbol{\sigma}}:\mathbf{S}^*:\overline{\boldsymbol{\sigma}}=-\frac{1}{2}\overline{\boldsymbol{\sigma}}:(v_f\mathbf{S}_f+v_m\mathbf{S}_m):\overline{\boldsymbol{\sigma}} \tag{2.5}$$

where $\mathbf{S}^*$ is the effective compliance tensor of the split specimen, v_f, v_m are volume fractions of fiber and matrix, respectively. The matrix volume fraction v_m is assumed throughout to be $(1-v_f)$.

The fiber and the matrix are assumed to be isotropic and the compliance tensor of fiber and matrix, $\mathbf{S}_f, \mathbf{S}_m$ can be expressed in terms of their respective Young's moduli (E_f, E_m) and Poisson's ratios (ν_f, ν_m). Therefore, the elastic energy density for the split specimen, E_s, is given as a quadratic form of the axial compressive stress, σ

[2]Expressions for $C_{11}^*, C_{12}^*, C_{22}^*, C_{23}^*$ are shown in the Appendix.

$$E_s = -\frac{1}{2}\overline{\boldsymbol{\sigma}}:(v_f \mathbf{S}_f + v_m \mathbf{S}_m):\overline{\boldsymbol{\sigma}}$$

$$= -\frac{1}{2}\left[\frac{v_f}{E_f}\{\sigma^2 - 4\nu_f\sigma\sigma_c + 2(1-\nu_f)\sigma_c^2\} + \frac{(1-v_f)}{E_m} \times\{\sigma^2 - 4\nu_m\sigma\sigma_c + 2(1-\nu_m)\sigma_c^2\}\right]. \quad (2.6)$$

The surface energy per unit volume, Γ, of the RVE due to splitting can be obtained by introducing a surface energy per unit area, γ

$$\Gamma = \frac{2\gamma A}{V} = \frac{2\gamma(2\pi a h)}{\pi R^2 h} = \frac{4\gamma v_f}{a} \quad (2.7)$$

where A is the lateral surface area of a fiber in the RVE, a is the radius of the fiber, and R is the radius of the RVE. Note that Γ (2.7) is independent of the height of the RVE, h, the height of the specimen. The surface energy γ can be interpreted as the energy release rate ($G_c = 2\gamma$) for interfacial crack initiation along the fiber-matrix interface or delamination ([19]) and the failure is assumed to proceed catastrophically following initiation ([20]). The relationship between the energy release rate G, and the local stress intensity factors K_{I} and K_{II} and the phase angle can be found in Liu et al. [19].

In the present analysis, the surface energy per unit area, γ, is assumed to be a constant (i.e., γ is independent of σ and σ_c). In reality, as confining pressure σ_c increases, the resistance to longitudinal (axial) splitting or delamination failure increases considerably and hence, the fracture energy, G_c or γ. Even though this appears to be consistent with what one might expect, nothing is known at present concerning the effect of pressure on fracture toughness of composite materials.

The total potential energy density of the split specimen, Π_s, is the sum of the elastic energy density, E_s and the surface energy density, Γ,

$$\Pi_s = E_s + \Gamma. \quad (2.8)$$

2.3 Criterion for Longitudinal Splitting. From the principle of minimum potential energy, the criterion for axial splitting can be expressed as

$$\Pi_u - \Pi_s < 0 \Rightarrow \text{unsplit} \quad (2.9a)$$

$$\Pi_u - \Pi_s = 0 \Rightarrow \text{neutral} \quad (2.9b)$$

$$\Pi_u - \Pi_s > 0 \Rightarrow \text{split}. \quad (2.9c)$$

Assuming that Γ is independent of stress state, the equipotential line $\Pi_u - E_s = \Gamma$, i.e., $\Pi_u - \Pi_s = 0$ provides the stress state for the neutral condition (2.9*b*). Examining the quadratic form $\Pi_u - E_s$, it can be shown that $\Pi_u - E_s$ is a monotonically increasing function of σ for $\sigma_c = constant$ provided $\sigma > \sigma_c$. Therefore, the critical condition is given by the equality

$$\Pi_u - \Pi_s = 0. \quad (2.10)$$

The criterion for longitudinal splitting (2.10) could be interpreted in terms of the surface energy of the newly created surfaces ($G_c = 2\gamma$) which cause the reduction in the elastic energy of the intact (unsplit) material.

3 Results

3.1 Compressive Strength. Substituting for Π_u and Π_s from (2.4) to (2.8), the critical stress for longitudinal splitting can be obtained by solving (2.10). Since the form of the total potential energy is a quadratic of σ, there are two roots σ_1 and σ_2:

$$\sigma_{1,2} = \frac{p_2\sigma_c \pm \sqrt{p_2^2\sigma_c^2 - p_1(p_3\sigma_c^2 - \Gamma)}}{p_1} \quad (3.1)$$

where p_1, p_2, and p_3 are expressed in terms of the elastic constants of the materials

$$p_1 = \frac{1}{2}\left(\frac{v_f}{E_f} + \frac{v_m}{E_m} - \frac{1}{E_1^*}\right), \quad p_2 = \frac{v_f\nu_f}{E_f} + \frac{v_m\nu_m}{E_m} - \frac{\nu_{21}^*}{E_1^*},$$

$$p_3 = \frac{v_f(1-\nu_f)}{E_f} + \frac{v_m(1-\nu_m)}{E_m} - \frac{1}{2}\left(\frac{1}{K_{23}^*} + \frac{4\nu_{21}^{*2}}{E_1^*}\right).$$

For a given confining pressure σ_c and surface energy density γ, $\sigma_1 \geqslant \sigma_2$, hence, σ_1 is taken as the critical stress σ^*. Letting $\sigma_c = 0$ in (3.1), the critical stress without confinement, i.e., the unconfined longitudinal compressive strength for the composite can be obtained:

$$\sigma^*|_{\sigma_c=0} = 2\left(\frac{2\gamma v_f}{a}\right)^{1/2}\left(\frac{v_f}{E_f} + \frac{v_m}{E_m} - \frac{1}{E_1^*}\right)^{-1/2}. \quad (3.2)$$

Equation (3.2) shows that unconfined strength is proportional to the square root of surface energy and inversely proportional to the square root of fiber diameter. This result indicates that for a given volume fraction, all other things remaining unchanged, composites with larger fiber diameter are more susceptible to axial splitting than smaller diameter fibers. Since $E_f \gg E_m$ in usual fiber-reinforced composites, $v_m/E_m \gg v_f/E_f$ and $E_1^* \cong v_f E_f$ hold. Based on these evaluations, (3.2) can be simplified as follows:

$$\sigma^*|_{\sigma_c=0} = 2\left(\frac{2\gamma v_f}{a}\right)^{1/2}\left(\frac{1-v_f}{E_m} - \frac{1}{v_f E_f}\right)^{-1/2}. \quad (3.3)$$

Examining the quadratic form of the energy surface, $\Phi(\sigma, \sigma_c) = \Pi_u - \Pi_s$ for a constant surface energy density γ, and assuming that the longitudinal (fiber direction) compliance is smaller than the lateral (transverse) compliance in the composite (typical for most fiber reinforced composites) the following inequality holds:

$$\frac{d\sigma^*}{d\sigma_c} \leqslant 1 \quad (3.4)$$

subject to the constraints

$$\sigma > \sigma_c \quad (3.5a)$$

and

$$d\Phi = \frac{\partial\Phi}{\partial\sigma}d\sigma + \frac{\partial\Phi}{\partial\sigma_c}d\sigma_c = 0. \quad (3.5b)$$

The first constraint (3.5*a*) corresponds to axial compression and the second constraint (3.5*b*) corresponds to the equi-potential line. From (3.4), one can conclude that if the splitting failure is governed by the principle of minimum total potential energy and the surface energy density γ is a constant, the slope of the relationship between compressive strength and confining pressure, i.e., σ^* versus σ_c, cannot exceed unity. Even if the surface energy density γ is an increasing function of confining pressure σ_c, the inequality (3.4) holds at least for small σ_c. The effect of lateral confinement and material properties on the compressive strength of composites can be investigated by using (3.1).

3.2 Model Predictions. Examining the functional form shown in (3.1) and (3.2), important parameters for longitudinal splitting can be identified as γ/a, v_f, and σ_c. To investigate the dependence of compressive strength on each of these parameters and compare the effect of each parameter, parametric studies have been performed. In the present parametric study, two different types of commonly used fiber-reinforced composite are investigated to illustrate the dependence of compressive strength on material properties. These materials are a unidirectional E-glass/vinylester composite (indicated as ''G/VE'' in the figures) and a unidirectional carbon/epoxy composite (indicated as ''C/ER'' in the figures). Experimental data and material properties for these materials are available in the literature ([11,15]). The relevant

Table 1 Material properties of fiber and matrix and geometry of fiber

	Fiber				Matrix		Interface
	E_f (GPa)	ν_f[(d)]	v_f	a (μm)	E_m (GPa)	ν_m	γ[(d)] (J/m^2)
E-Glass/Vinylester	72.4[(a)]	0.2	0.1−0.6[(a)]	12.1[(a)]	3.69[(a)]	0.38[(d)]	110,210
Carbon/Epoxy	260[(b)]	0.2	0.36[(b)]	3.4[(b)]	1.63[(b)]	0.34[(b)]	140
Carbon/Epoxy	234[(c)]	0.2	0.6[(c)]	3.4[(d)]	4.28[(c)]	0.34[(d)]	140

[(a)]Waas et al. [15];
[(b)]Weaver and Williams [10];
[(c)]Parry and Wronski [11];
[(d)]assumed

material properties including those of the fiber and the matrix as well as the radius of the fibers for these composites are shown in Table 1. Surface energy density γ's shown in Table 1 are obtained by calibration to the corresponding experimental data for unconfined compressive strength.

Figure 2 shows the compressive strength of two types of composite for different γ/a and σ_c (0 and 100 MPa) with fixed fiber volume fraction $v_f=60$ percent. One can observe a strong dependence of compressive strength on γ/a (proportional to $\sqrt{\gamma/a}$) and relatively weak dependence on σ_c. Also, the compressive strength seems to be almost insensitive to the choice of the material for a given value of γ/a. Small values of γ/a correspond to low interfacial energy (weak interface) and/or large diameter fibers, whereas large values of γ/a correspond to large interfacial energy (tough interface) and/or small diameter fibers. The unconfined compressive strengths of E-glass/vinylester composite and carbon/epoxy composite with $v_f=60$ percent are 667 MPa [15] and 1.5 GPa ([11]), respectively. Based on these experimental observations, if the v_f is identical, the carbon/epoxy composite appears to be stronger than the E-glass/vinylester composite. However, the strong dependence on γ/a plays a significant role here. Suppose γ is of the same order for both composites, fiber radii a for E-glass/vinylester composite and carbon/epoxy composite are 12.1 μm and 3.4 μm, respectively (see Table 1). This results in γ/a for the carbon/epoxy composite to be approximately four times as that of the E-glass/vinylester composite.

Figure 3 shows unconfined compressive strength (i.e., $\sigma_c=0$) as a function of γ/a and v_f. For a given γ/a, effect of v_f on compressive strength is much stronger than that of the material properties. This observation together with the insensitivity of the strength to the choice of the material observed in Fig. 2 has the following implication. The compressive strength of the unidirectional fiber-reinforced composite is relatively insensitive to the magnitude of the material properties of each constituent, i.e., fiber and matrix. Instead, the degree of anisotropy introduced by combining the materials with different material properties is an important factor in the determination of compressive strength. Longitudinal splitting can be considered to be the process in which excessive stored elastic energy due to the heterogeneity and anisotropy can be released through the formation of new surfaces. The importance of anisotropy has been evidenced in this parametric study.

Compressive strength for different v_f and σ_c with fixed γ/a is shown in Fig. 4. Based on experimental observations, $\gamma/a=1.32\times10^7$ J/m^3 and $\gamma/a=4.17\times10^7$ J/m^3 are used for E-glass/vinylester and carbon/epoxy, respectively, as the best fitting values for the model prediction of their unconfined compressive strength ([11,15]). It is again seen that if the same values for γ/a were used, the compressive strength for both materials are close to each other as expected from previously shown parametric studies (Figs. 2 and 3). In this case, the difference between the results for two different levels of confinement $\sigma_c=0$ MPa $\sigma_c=100$ MPa is small and nearly constant for all values of v_f shown here. This shows that the effect of σ_c on compressive strength is much weaker than that of v_f and is relatively insensitive for a given v_f.

3.3 Comparison With Experiments. To verify the validity of the energy-based model for longitudinal splitting, the compressive strengths predicted by the present model are compared with the experimental results obtained for E-glass/vinylester and carbon/epoxy composites. Uniaxial compression tests on unidirectional fiber-reinforced E-glass/vinylester composite with different fiber volume fraction ranging from 0 percent to 60 percent were performed by Waas et al. [15]. For carbon/epoxy composites, compression tests on unidirectional fiber-reinforced composites under superposed hydrostatic confinement have been performed

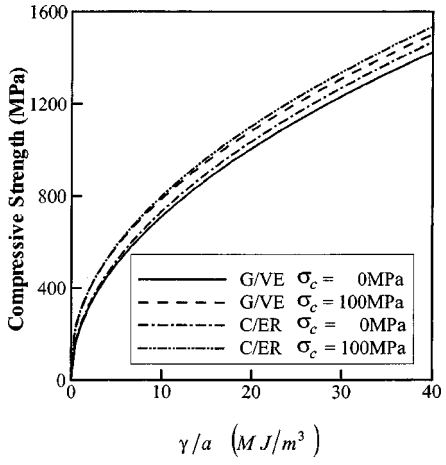

Fig. 2 Effect of surface energy and lateral confinement on compressive strength (G/VE stands for E-Glass/vinylester and C/ER stands for carbon/epoxy)

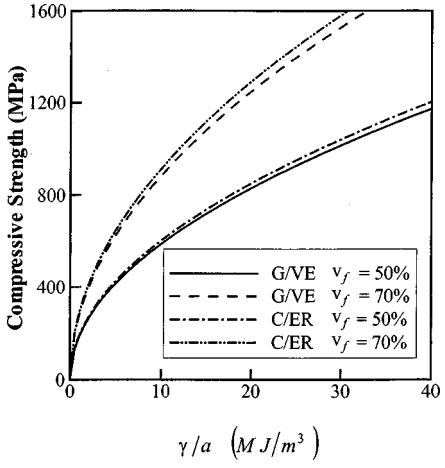

Fig. 3 Effect of surface energy and fiber volume fraction on unconfined compressive strength ($\sigma_c=0$) (G/VE stands for E-Glass/vinylester and C/ER stands for carbon/epoxy)

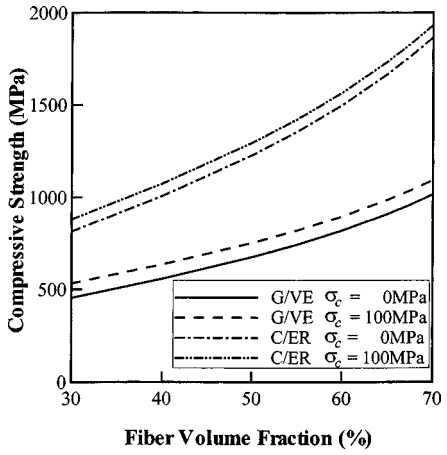

Fig. 4 Effect of fiber volume fraction and lateral confinement on compressive strength (G/VE stands for E-Glass/vinylester and C/ER stands for carbon/epoxy)

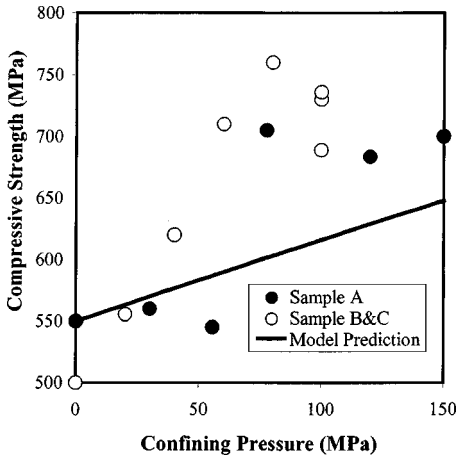

Fig. 6 Comparison between experimental results ([10]) and model prediction for carbon/epoxy composite, v_f=36 percent

by Weaver and Williams [10] and Parry and Wronski [11]. The input parameters for the model prediction including material properties, fiber radius, and surface energy of the material used in their experiments have been shown in Table 1.

Comparison between the model prediction and experimental results by Waas et al. [15] provides the measure of the validity of the present model with respect to changing v_f. Experimental results for the unconfined compressive strength from Waas et al. [15] are shown in Fig. 5. Examining the trend in compressive strength, one can observe a dip between $v_f=30$ percent and $v_f=40$ percent. Based on this observation, analysis is performed for two groups of data sets. One is for low v_f, i.e., $v_f \leqslant 30$ percent, the other is for high v_f, i.e., $v_f \geqslant 40$ percent. Only the difference in these analyses is the input parameter for the surface energy γ. The values of the surface energy which enable the model predictions to show good agreement with experimental results are $\gamma=210$ J/m^2 for the low v_f data set and $\gamma=110$ J/m^2 for the high v_f data set. In the present model, γ has been assumed to be the surface energy associated with delamination between the fiber and the matrix. The surface energy associated with the creation of new surfaces in the matrix has been neglected. In the case of high v_f, surface energy associated with matrix failure is negligible since the average distance between fibers is small and the area of the surface created by matrix failure is much smaller than the one created by interface (fiber-matrix) debonding. On the other hand, as the fiber volume fraction decreases, the average distance between fibers increases and the surface energy associated with matrix failure becomes no longer negligible, which results in the increase of total surface energy. Also, the nonlinearity of the matrix for vinylester ([15]) which is important at low volume fractions of the fiber has been neglected in the present analysis. The increase in surface energy associated with matrix failure is consistent with the requirement for larger surface energy γ for lower v_f. Further work towards quantification of fracture energies as a function of volume fraction in fiber reinforced composites is needed. The model predictions for the matrix-dominated region and the fiber-interface dominated region can be regarded, respectively, as upper and lower bound for compressive strength of the composite.

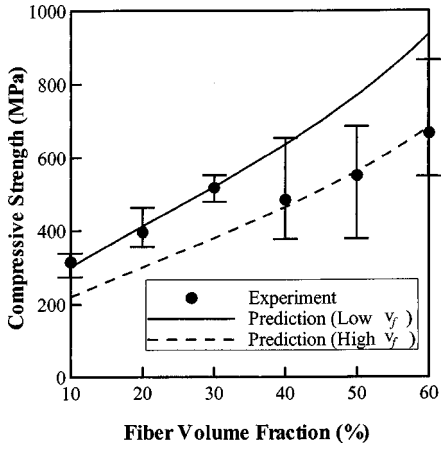

Fig. 5 Comparison between experimental results ([15]) and model predictions for E-Glass/vinylester composite

The experimental result shows considerable scatter for $v_f \geqslant 40$ percent. In general, the interfacial toughness is highly dependent on local conditions such as size/orientation of initial imperfection, mode mixity, and bonding (interface strength and toughness). As a result, the interface properties vary more than the material properties of each constituent of composite, i.e., fiber and matrix. The fracture energy of fiber-reinforced composites (G_c) depends strongly on the local mode mixity ([19]). Therefore, for the case of low v_f, the scatter in compressive strength is relatively small since the matrix plays a signifiant role in determining the surface energy associated with splitting. On the other hand, since the surface energy associated with fiber/matrix debonding is dominant for high v_f, the local interfacial conditions play a significant role in determining the compressive strength. This results in a large scatter of the compressive strength for composites with high v_f as seen from the experimental results in Fig. 5.

Comparison between the model prediction and experimental results by Weaver and Williams [10] (WW) and Parry and Wronski [11] (PW) provides a measure of the validity of the present model with respect to the confining pressure, σ_c. To the best knowledge of the authors, WW and PW are the most widely accepted reliable experimental data regarding compressive failure of unidirectional fiber-reinforced composites under superposed hydrostatic confinement including detailed discussion on failure modes. Although some specimen geometry dependence of failure mode is reported in PW and short specimens used in WW show end effect, their experiments are convincing enough to regard longitudinal splitting as the dominant failure mode under weak lateral confinement. The critical stress σ^* is plotted against the confining pressure σ_c in Fig. 6 (WW for $0 \leqslant \sigma_c \leqslant 150$ MPa) and in Fig. 7 (PW for $0 \leqslant \sigma_c \leqslant 300$ MPa). In the experiments by PW, for higher confining pressure ($\sigma_c > 150$ MPa), the slope of σ_c versus σ^* graph is steeper than those for lower confining pressure as seen in Fig. 7.

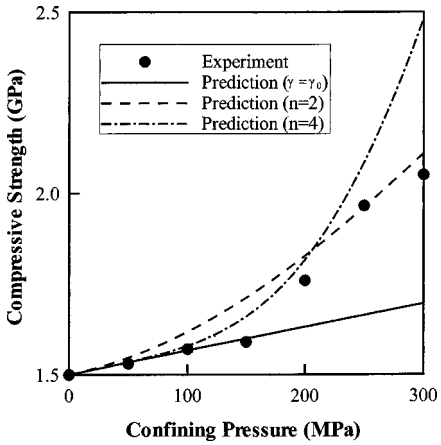

Fig. 7 Comparison between experimental results ([11]) and model predictions with the effect of increasing surface energy for carbon/epoxy composite, $vf=60$ percent

This increase of the slope is also observed in the experiments by WW. Besides, both observed failure mode transition from longitudinal splitting to kink banding around $\sigma_c = 150$ MPa. Therefore, the comparisons are restricted to low levels of confinement, i.e., $0 \leqslant \sigma_c \leqslant 150$ MPa. Surface energy per unit area, γ, used here is assumed to be the same for both the cases and is shown in Table 1. The model predictions show significant agreement with the experimental results, especially with those obtained by PW (Fig. 7). The theoretical predictions agree with the experimental results given by WW (Fig. 6) for confining pressures $0 \leqslant \sigma_c \leqslant 50$ MPa. However, in the range of $50 \leqslant \sigma_c \leqslant 150$ MPa, the agreement is not good. The experimental results show considerable scatter for confining pressures $50 \leqslant \sigma_c \leqslant 150$ MPa although the samples A, B, and C are made of the same material. It is believed that due to low fiber volume fraction (36 percent), a host of failure modes might have occurred under the confining pressure $50 \leqslant \sigma_c \leqslant 150$ MPa in the experiments by WW, and this could explain the scatter in experimental results. Also, $v_f = 36$ percent happens to be in the range of transition zone from matrix-dominated region to interface dominated region for longitudinal (axial) splitting of E-glass/vinylester composite discussed above. Although the material is different, the geometrical interpretation about the increase of the area of the matrix failure still holds in this case. Therefore, the large scatter in compressive strength might be a result of the characteristic of the transition zone between low and high volume fraction of fibers.

In the present model, the only adjustable parameter is surface energy per unit area, γ, which is not readily available for the composites considered here from experimental measurements. However, the values γ used in the model predictions appear to be consistent with data available for similar composite materials ([21]) by assuming $G_c = 2\gamma$.

4 Conclusions and Discussion

An energy-based model has been developed for predicting the compressive strength of unidirectional fiber-reinforced composites which fail by longitudinal (axial) splitting. The following conclusions are based on the analytic results (3.1) and (3.2):

(i) The critical stress for longitudinal splitting is proportional to $\sqrt{\gamma/a}$ and this parameter is the most dominant term in the determination of the compressive strength of fiber-reinforced composites. According to the present model, composites with larger fracture energy and small fiber diameters would result in higher strength.

(ii) The degree of the anisotropy plays a significant role and the effect of fiber volume fraction appears only in this context in influencing the compressive strength.

(iii) The effect of confining pressure on compressive strength is relatively weak.

The model prediction has been compared with the experimental results and showed good agreement. This agreement supports the validity of the present method for the analysis of longitudinal splitting (delamination failure) in unidirectional fiber-reinforced composites.

The assumption of a constant γ would predict longitudinal splitting at all levels of confinement and with markedly lower strength than experimentally observed ones at high confining pressures. Beyond certain confining pressure, longitudinal splitting is completely suppressed and the failure mode translates to kink banding ([10–12]). In order to illustrate the effect of increasing fracture surface energy γ with increasing pressure, γ is assumed to depend on σ_c as follows:

$$\gamma = \gamma_0 \left\{ 1 + \alpha_n \left(\frac{\sigma_c}{\sigma_0^*} \right)^n \right\} \tag{4.1}$$

where γ_0 is surface energy for $\sigma_c = 0$, σ_0^* is the unconfined compressive strength, n is the confining pressure hardening exponent, and α_n is a positive dimensionless parameter corresponding to the exponent n. For $n \neq 0$ in (4.1), γ increases as σ_c increases and this results in nonlinear dependence of model prediction of compressive strength on σ_c. In this case, the inequality (3.4) for the slope of σ^* versus σ_c being less than unity holds at least for small σ_c. The dependence of γ on σ_c (4.1) can be viewed to reflect the increase in the energy release rate G_c as the local mode-mixity for interface cracking changes from mostly mode I to mode II ([19]) with increasing confinement.

The model predictions of compressive strength for the carbon/epoxy composite used by Parry and Wronski [11] for the cases $n=2$ and $n=4$ in (4.1) are shown in Fig. 7. Input parameters for the model predictions are $\gamma_0 = 140$ J/m^2, $\sigma_0^* = 1.5$ GPa, $\alpha_2 = 15.58$, and $\alpha_4 = 823.6$. Comparison between the cases of $n=2$ and $n=4$ shows that as the exponent n increases, the curvature of the failure envelope can be increased and as a result, the model prediction for longitudinal splitting stays close to experimental result in wider range of confinement than the prediction based on smaller n and exceeds the experimental value at high confining pressures where formation of kink bands, instead of longitudinal splitting, is observed in experiments. This observation implies that if γ increases as a function of σ_c and its dependence on σ_c is strong, i.e., exponent n is large, longitudinal or axial splitting can be observed up to certain levels of confinement and is suppressed at high levels of confinement where other failure modes such as kink band formation should be considered.

Acknowledgment

This work was supported by the Office of Naval Research (Dr. Y. D. S. Rajapakse, Scientific Officer) through a grant to the California Institute of Technology.

Appendix

Following Hashin and Rosen [16], the expression for the effective moduli of the unidirectional fiber composite (x_1-fiber direction) E_1^*, ν_{21}^*, K_{23}^*, and G_{23}^* are given below:

$$E_1^* = (v_f E_f + v_m E_m) \frac{E_m(D_1 - D_3 F_1) + E_f(D_2 - D_4 F_2)}{E_m(D_1 - D_3) + E_f(D_2 - D_4)},$$

$$\nu_{21}^* = \frac{v_f E_f L_1 + v_m E_m L_2 \nu_m}{v_f E_f L_3 + v_m E_m L_2}$$

$$K_{23}^* = K_m \frac{K_f(1 + 2\nu_m v_f) + 2K_m \nu_m v_m}{K_f v_m + K_m(v_f + 2\nu_m)};$$

$$G_{23}^{*}=G_m \Big/ \left[1+\frac{2(1-\nu_m)}{1-2\nu_m}v_f A_4\right] \quad \text{(lower bound)}$$

where $D_1=1-\nu_f$, $D_2=(1+v_f)/v_m+\nu_m$, $D_3=2\nu_f^2$, $D_4=2\nu_m^2 v_f/v_m$,

$$F_1=\frac{\nu_m v_f E_f+\nu_f v_m E_m}{\nu_f v_f E_f+\nu_m v_m E_m}, \quad F_2=\frac{\nu_f}{\nu_m}F_1,$$

$$L_1=2\nu_f(1-\nu_m^2)v_f+\nu_m(1+\nu_m)v_m, \quad L_2=v_f(1-\nu_f-2\nu_f^2),$$

$$L_3=2(1-\nu_m^2)v_f+(1+\nu_m)v_m,$$

$$\begin{aligned}A_4=&2(G_f-G_m)(2\nu_m-1)[G_m(4\nu_f-3)(v_f^3-1)\\&-G_f\{(4\nu_m-3)\nu_f^3-1\}]/[G_m^2(4\nu_f-3)(v_f-1)^4\\&-2G_fG_m\{-5+6\nu_m-4\nu_f+6v_f^2-4\nu_m v_f^3+(3-2\nu_m)\nu_f^4\\&+2\nu_f(3-4\nu_m+4v_m-6v_f^2+4\nu_m v_f^3-v_f^4)\}\\&+G_f^2\{3+4v_f-6v_f^2+4v_f^3(3-6\nu_m+4\nu_m^2)\\&+(3-4\nu_m)v_f^4-\nu_m\}]\end{aligned}$$

E_f, ν_f, v_f and E_m, ν_m, v_m are the Young's moduli, Poisson's ratios, and the volume fractions of the fiber and the matrix, respectively.

The elastic moduli $C_{11}^{*},C_{12}^{*},C_{22}^{*},C_{23}^{*}$ are expressed using E_1^{*}, ν_{21}^{*}, K_{23}^{*}, and G_{23}^{*} given above;

$$C_{11}^{*}=E_1^{*}+4\nu_{21}^{*2}K_{23}^{*}$$

$$C_{12}^{*}=2\nu_{21}^{*}K_{23}^{*}$$

$$C_{22}^{*}=K_{23}^{*}+G_{23}^{*}$$

$$C_{23}^{*}=K_{23}^{*}-G_{23}^{*}.$$

References

[1] Shuart, M. J., 1989, ''Failure of Compression-Loaded Multidirectional Composite Laminates,'' AIAA J., **27**, pp. 1274–1279.

[2] Waas, A. M., and Schultheisz, C. R., 1996, ''Compressive Failure of Composites, Part II: Experimental Studies,'' Prog. Aerosp. Sci., **32**, pp. 43–78.

[3] Fleck, N. A., 1997, ''Compressive Failure of Fiber Reinforced Composites,'' Adv. Appl. Mech., **33**, pp. 43–117.

[4] Tsai, S. W., and Wu, E. M., 1971, ''A General Theory of Strength for Anisotropic Materials,'' J. Compos. Mater., **5**, pp. 58–80.

[5] Christensen, R. M., 1997, ''Stress Based Yield/Failure Criteria for Fiber Composites,'' Int. J. Solids Struct., **34**, pp. 529–543.

[6] Budiansky, B., and Fleck, N. A., 1993, ''Compressive Failure of Composites,'' J. Mech. Phys. Solids, **41**, pp. 183–211.

[7] Kyriakides, S., Arseculeratne, R., Perry, E. J., and Liechti, K. M., 1995, ''On the Compressive Failure of Fiber Reinforced Composites,'' Int. J. Solids Struct., **32**, pp. 689–738.

[8] Schultheisz, C. R., and Waas, A. M., 1996, ''Compressive Failure of Composites, Part I: Testing and Micromechanical Theories,'' Prog. Aerosp. Sci., **32**, pp. 1–42.

[9] Lee, S. H., and Waas, A. M., 1999, ''Compressive Response and Failure of Fiber Reinforced Unidirectional Composites,'' Int. J. Fract., **100**, pp. 275–306.

[10] Weaver, C. W., and Williams, J. G., 1975, ''Deformation of a Carbon-Epoxy Composite Under Hydrostatic Pressure,'' J. Mater. Sci., **10**, pp. 1323–1333.

[11] Parry, T. V., and Wronski, A. S., 1982, ''Kinking and Compressive Failure in Uniaxially Aligned Carbon Fibre Composite Tested Under Superposed Hydrostatic Pressure,'' J. Mater. Sci., **17**, pp. 893–900.

[12] Sigley, R. H., Wronski, A. S., and Parry, T. V., 1992, ''Axial Compressive Failure of Glass-Fibre Polyester Composites Under Superposed Hydrostatic Pressure: Influence of Fibre Bundle Size,'' Compos. Sci. Technol., **43**, pp. 171–183.

[13] Bhattacharya, K., Ortiz, M., and Ravichandran, G., 1998, ''Energy-Based Model of Compressive Splitting in Heterogeneous Brittle Solids,'' J. Mech. Phys. Solids, **46**, pp. 2171–2181.

[14] Hashin, Z., 1996, ''Finite Thermoelastic Fracture Criterion With Application to Laminate Cracking Analysis,'' J. Mech. Phys. Solids, **44**, pp. 1129–1145.

[15] Waas, A. M., Takeda, N., Yuan, J., and Lee, S. H., 1997, ''Static and Dynamic Compressive Behavior of Glass Fiber Reinforced Unidirectional Composites,'' *Proceedings of the American Society for Composites, Twelfth Technical Conference*, Dearborn, MI, Technomic, Lancaster, PA, pp. 552–561.

[16] Hashin, Z., and Rosen, B. W., 1964, ''The Elastic Moduli of Fiber-Reinforced Materials,'' ASME J. Appl. Mech., **31**, pp. 223–232.

[17] Hill, R., 1964, ''Theory of Mechanical Properties of Fibre-Strengthened Materials: I. Elastic Behavior,'' J. Mech. Phys. Solids, **12**, pp. 199–212.

[18] Nemat-Nasser, S., and Hori, M., 1993, *Micromechanics: Overall Properties of Heterogeneous Materials*, Elsevier, New York.

[19] Liu, C., Huang, Y., Lovato, M. L., and Stout, M. G., 1997, ''Measurement of the Fracture Toughness of a Fiber-Reinforced Composite Using the Brazilian Disk Geometry,'' Int. J. Fract., **87**, pp. 241–263.

[20] Lambros, J., and Rosakis, A. J., 1997, ''Dynamic Crack Initiation and Growth in Thick Unidirectional Graphite/Epoxy Plates,'' Compos. Sci. Technol., **57**, pp. 55–65.

[21] Daniel, I. M., and Isahi, O., 1994, *Engineering Mechanics of Composite Materials*, Oxford University Press, Oxford, UK.